
A FULLY BAYESIAN GRADIENT-FREE SUPERVISED DIMENSION REDUCTION METHOD USING GAUSSIAN PROCESSES

A PREPRINT

Raphaël Gautier^{1*}, Piyush Pandita², Sayan Ghosh², and Dimitri Mavris¹

¹Aerospace Systems Design Laboratory, Georgia Institute of Technology, Atlanta, GA, 30332

²Probabilistic Design, GE Research, Niskayuna, NY, 12309

December 22, 2024

ABSTRACT

Modern day engineering problems are ubiquitously characterized by sophisticated computer codes that map parameters or inputs to an underlying physical process. In other situations, experimental setups are used to model the physical process in a laboratory, ensuring high precision while being costly in materials and logistics. In both scenarios, only limited amount of data can be generated by querying the expensive information source at a finite number of inputs or designs. This problem is compounded further in the presence of a high-dimensional input space. State-of-the-art parameter space dimension reduction methods, such as active subspace, aim to identify a subspace of the original input space that is sufficient to explain the output response. These methods are restricted by their reliance on gradient evaluations or copious data, making them inadequate to expensive problems without direct access to gradients. The proposed methodology is gradient-free and fully Bayesian, as it quantifies uncertainty in both the low-dimensional subspace and the surrogate model parameters. This enables a full quantification of epistemic uncertainty and robustness to limited data availability. It is validated on multiple datasets from engineering and science and compared to two other state-of-the-art methods based on four aspects: a) recovery of the active subspace, b) deterministic prediction accuracy, c) probabilistic prediction accuracy, and d) training time. The comparison shows that the proposed method improves the active subspace recovery and predictive accuracy, in both the deterministic and probabilistic sense, when only few model observations are available for training, at the cost of increased training time.

Keywords surrogate modeling, high-dimensional input space, dimensionality reduction, uncertainty quantification, active subspace, Bayesian inference, Gaussian process regression

1 Introduction

Engineering problems, with high-dimensional inputs or parameters, are often modeled in the form of expensive computer codes or expensive laboratory experiments. These scenarios severely limit the number of data, namely input-output pairs, that can be observed. This requires developing inexpensive surrogate models that a) accurately model the underlying physical process and b) quantify the epistemic uncertainty due to limited observed data. Once an accurate and reliable surrogate is developed with quantification of uncertainty, it can be used to learn arbitrary statistics about the output [1], generate more data intelligently [2, 3] and make predictions under a limited budget [4].

In the context of data-driven probabilistic surrogate modeling, the curse of dimensionality remains a major obstacle in the way of developing a surrogate that is accurate and can help infer meaningful statistics about the output. High dimensionality may be encountered in the input, state, and output spaces, or any combination thereof. High dimensionality of the state and output spaces has been the subject of extensive research in the fields of reduced-order

*raphael.gautier@gatech.edu

modeling and equation-free model reduction [5]. As a result, data-fit and physics-based surrogates of high-dimensional responses are now widespread in the literature. They leverage unsupervised methods, such as principal component analysis (PCA) [6], deep autoencoder-decoder networks [7], or diffusion maps [8]. These methods are not directly applicable to the problem of high-dimensional *input* spaces, as they do not take the response into account when learning the dimension reduction transformation. They may therefore lead to sub-optimal performance as they discard information that is useful for predicting the response of interest. Reduction of the input space dimension demands a thorough understanding of the relationship between the inputs and the underlying function. As recognized in [9], supervised techniques bring an advantage over unsupervised methods when applied in the context of surrogate modeling. For some meta-modeling methods, an increase in input dimensionality may quickly lead to a prohibitively high number of required model evaluations [10]. Among possible routes for identifying the lower-dimensional representation, the two deemed most promising in literature are: a) mapping strategies that take advantage of the dependence on low-dimensional manifolds instead of the original high-dimensional space, and b) lower-dimensional models, and in particular additive or partially additive models, which are motivated by many observations that high-order interactions are negligible in most scientific and engineering problems, e.g. high-dimensional model representation [11]. The method proposed in this work belongs to the first category.

While mapping strategies are a broad denomination proposed in [12] in the context of engineering design, similar methods actually exist under other names in other fields: ridge functions in the function approximation literature [13, 14, 15, 16, 17, 18, 19, 20, 21, 22, 23], sufficient dimension reduction [24, 25, 26, 27, 28], spectral methods, sometimes referred to as supervised dimension reduction or dimension reduction for supervised learning [29, 30, 31, 32, 33, 34], or probabilistic approaches [35, 36]. These methods aim at similar objectives while leveraging different mathematical tools. The term ridge function is usually used to refer to functions obtained by mapping the original high-dimensional space onto a low-dimensional subspace and extensive literature on this topic can be found. Recent methods were proposed to identify ridge functions, that either rely on sparse matrix approximations [23, 37] or low-rank approximations [21, 22]. The sparse approximation is hard to justify, as there is no theoretical argument to back the fact that the covariance matrix of the gradient is sparse. Low-rank approximation methods can be interpreted as approximating finite-difference gradients, which is very ineffective and hinders exploration of the full input space by requiring many model evaluations around a limited number of points. In the sufficient dimension reduction literature [26, 38], methods such as sliced inverse regression [38] have been extensively used. However, as they assume elliptical distribution for the parameters, they do not fit the needs encountered when generating surrogate models, where the input space is usually uniformly sampled. Hessian-based approaches have also been proposed to identify low-dimensional manifolds in the input space [39]. It is also interesting to note that while we are seeking methods that provide an explicit two-way mapping between the low- and high-dimensional spaces, the success of recent deep learning techniques can be attributed to an implicit dimensionality reduction, referred to as feature extraction [40].

The gradient-based active subspace (AS) method [41] is among the most recent additions to the mapping or projection-based strategies. It has shown considerable promise on challenging engineering applications [42, 43, 44, 45, 46, 47]. Extensions of the method to multivariate outputs [48, 49] and to the multi-fidelity setting [50] are the subject of ongoing research. Similar ideas were also independently pursued [51, 52]. While AS is in practice restricted to problems for which adjoint derivatives can be obtained, alternative formulations have been proposed to identify the low-dimensional structure of the input space using direct function evaluations only. To that end, some methods combine the projection onto the AS with a probabilistic surrogate model such as Gaussian process (GP) regression [35, 53, 49]. However, they only partially quantify epistemic uncertainty, as the projection matrix on the AS results from an optimization process instead of a Bayesian inference process. While similar approaches have been taken for other kinds of surrogates [54, 36, 9], the fully Bayesian inference of the projection matrix combined with a Gaussian process surrogate has not yet been attempted. Such an approach would open the door to efficient meta-modeling for high-dimensional problems using GPs, including a full quantification of epistemic uncertainty.

A difficulty resides in the presence of an orthonormal projection matrix in the model. Readily available Markov chain Monte-Carlo (MCMC) samplers operate in Euclidean space, as model parameters usually encountered in Bayesian inference are real-valued. Methods to apply MCMC to orthogonal matrices have been developed following two different approaches: Riemannian Hamiltonian Monte-Carlo (RHMC) techniques [55, 56] and re-parametrization techniques [57, 58, 59, 60]. The formers modify the leapfrog steps of the original Hamiltonian Monte-Carlo (HMC) algorithm to ensure that the new proposals remain on the Stiefel manifold, i.e. the manifold of orthogonal matrices. The orthogonality constraint is therefore satisfied by construction. The latter simply use parameterization techniques, such as Householder reflections [58], polar angles [59], the Givens representation [60], or simply using the Gram-Schmidt orthogonalization algorithm [61], in order to transform a set of scalar parameters into an orthogonal matrix. While RHMC methods are theoretically elegant and lie on strong mathematical foundations, they require the implementation of specialized MCMC samplers [62]. “Turn-key” MCMC algorithms that do not require extensive tuning have not yet been developed for RHMC. As a consequence, implementations and usages of these methods are still at a very

early stage of research. The method recently proposed in [63] is representative of such approaches. On the other hand, reparameterization approaches can be used with most of the openly-available MCMC samplers [57, 58, 59, 60]. These methods have been leveraged in instances where orthogonal matrices were part of the probabilistic model. In these applications, inference on orthogonal matrices was successfully carried out. However, these methods have not yet been applied to the fully Bayesian inference of the AS. In this work, we employ reparameterization methods on the projection matrix to obtain matrices in the Stiefel manifold. This allows us to leverage existing MCMC algorithms to quantify uncertainty on both the parameters of the projection matrix onto the AS and the hyperparameters of the Gaussian process.

Multiple contributions are made in this paper. The first contribution is a fully Bayesian and gradient-free formulation for meta-modeling of functions with high-dimensional inputs drawing inspiration from the AS method. Under this formulation, all model parameters are considered uncertain, including those associated with the projection onto the lower-dimensional input subspace. The second contribution is a set of algorithms that enable the practical implementation of the proposed formulation using “turn-key” MCMC samplers. Those additional implementation specifics, based on Householder transforms, are needed to simultaneously accommodate traditional GP hyperparameters defined in Euclidean space and an orthonormal projection matrix belonging to the Stiefel manifold as model parameters during probabilistic inference. The third contribution is a thorough comparative study of the model’s performance with two recently proposed methods as seen from four different perspectives. The last contribution is a repository, written in the Python programming language and made openly available, that implements the proposed algorithms and benchmark methods using state-of-the-art probabilistic programming languages, manifold optimization libraries, and computational backends, enabling reproducibility and allowing interested researchers to develop extensions to the proposed method.

The outline of the rest of the paper is as follows. Our methodology is summarized in section 2. In particular, subsection 2.5 introduces the method and algorithms proposed to parameterize the projection matrix and the fully Bayesian inference algorithm. In section 3, we demonstrate the performance of the methodology through numerical experiments on eight analytical functions of 25 to 100 inputs and four science and engineering datasets with input dimensions ranging from 18 to 100. Since computationally expensive analyses highly constrain the number of observations available to train the surrogate model, the impact of the training set size on all metrics of interest is systematically assessed. Finally, we summarize our findings in section 4 and discuss natural extensions of the methodology to be explored next.

2 Methodology

This section is organized as follows. Notation is first introduced in section 2.1. Background methods are then briefly summarized: Gaussian process regression in section 2.2, active subspace in section 2.3, and gradient-free active subspace using Gaussian processes in section 2.4. Finally, the proposed fully Bayesian method is detailed in section 2.5.

2.1 Notation

Let f be the mapping through which we collect data about the underlying physical process of interest. We assume that f is a scalar-valued function of d variables. High-dimensional input spaces, i.e. large d , are the focus of this study.

$$\begin{aligned} f : \mathcal{X} \subseteq \mathbb{R}^d &\rightarrow \mathcal{Y} \subseteq \mathbb{R} \\ \mathbf{x} &\rightarrow y = f(\mathbf{x}) \end{aligned} \quad (1)$$

We assume that a total of n input-output pairs, or model observations, have been obtained by evaluating the model f at the input sites $\mathbf{x}_1, \dots, \mathbf{x}_n$ and are available to support the creation of the surrogate model. Following standard practices, we partition model observations into a training set \mathcal{D} of size p and a validation set \mathcal{D}_* of size q such that $p + q = n$. In the context of surrogate modeling, the observations in \mathcal{D} are used for training the model while those in \mathcal{D}_* allow to assess the performance of the predictive model.

$$\mathcal{D} = \{(\mathbf{x}_i, y_i) \mid i = 1, \dots, p\} \quad (2)$$

$$\mathcal{D}_* = \{(\mathbf{x}_i^*, y_i^*) \mid i = 1, \dots, q\} \quad (3)$$

Let $\mathbf{X} = [\mathbf{x}_1, \dots, \mathbf{x}_p]^T$ and $\mathbf{X}_* = [\mathbf{x}_1^*, \dots, \mathbf{x}_q^*]^T$ respectively be the $p \times d$ and $q \times d$ design matrices corresponding to the training and validation input sites. Accordingly, let \mathbf{y} and \mathbf{y}_* be the size p and q training and validation response vectors. We focus on the creation of a surrogate model \hat{f} of f such that \hat{f} can be evaluated in lieu of f . We work within the probabilistic framework to quantify uncertainty in the surrogate model predictions. As such, we are seeking a generative model, i.e. a model for the joint probability distribution $p(\mathbf{X}, \mathbf{y})$. Probabilistic predictions for points in the validation set can then be made by using the conditional predictive distribution $p(\mathbf{y}_* | \mathbf{X}_*, \mathbf{X}, \mathbf{y})$.

2.2 Gaussian Process Regression

Gaussian process regression (GPR) is a popular surrogate modeling method that grants access to predictive uncertainty. We briefly recall the main results behind GPR, mostly adopting the reference notation introduced in [64]. The GPR model relies on the assumption that the prior distribution for the underlying mapping f can be modelled as a GP: for a set of latent, unobserved, model responses made at input sites \mathbf{X} and arranged in the vector \mathbf{f} , there exist a vector μ and a matrix Σ such that $\mathbf{f} \sim \mathcal{N}(\mu, \Sigma)$. Additionally, it is assumed that observations \mathbf{y} of \mathbf{f} are uncertain, such that $\mathbf{y} \sim \mathcal{N}(\mathbf{f}, \sigma_n)$. Those assumptions enable the analytical marginalization of the latent vector \mathbf{f} , leading to the following prior distribution for the observations: $\mathbf{y} \sim \mathcal{N}(\mu, \Sigma + \sigma_n \mathbf{I})$.

Multiple options for constructing the mean vector μ and the covariance matrix Σ exist and lead to different GPR variants. Common assumptions are made in this work. First, we assume the model observations to be centered and the mean of the prior GP to be zero, i.e. $\mu = [0, \dots, 0]^T$. Then, a kernel function k is used to construct Σ by encoding the correlation structure of the GP, i.e. the correlation between responses y and y' at input locations \mathbf{x} and \mathbf{x}' . We use the widespread automatic relevance determination (ARD) kernel:

$$k(\mathbf{x}, \mathbf{x}') = \sigma_f \prod_{i=1}^d \exp\left(-\frac{(x_i - x'_i)^2}{2\ell_i^2}\right) \quad (4)$$

where σ_f is the signal variance and $\ell = [\ell_1, \dots, \ell_d]$ are characteristic length scales. For convenience, we denote as K the generalization of the kernel function k to design matrices. For two design matrices \mathbf{X} and \mathbf{X}' respectively containing n and n' points, we have:

$$K(\mathbf{X}, \mathbf{X}') = \begin{bmatrix} k(\mathbf{x}_1, \mathbf{x}'_1) & \dots & k(\mathbf{x}_1, \mathbf{x}'_{n'}) \\ \vdots & \ddots & \vdots \\ k(\mathbf{x}_n, \mathbf{x}'_1) & \dots & k(\mathbf{x}_n, \mathbf{x}'_{n'}) \end{bmatrix} \quad (5)$$

Using that notation, the GP covariance matrix is then computed as $\Sigma = K(\mathbf{X}, \mathbf{X})$. We gather all hyperparameters into the vector $\theta = [\sigma_n, \sigma_f, \ell_1, \dots, \ell_d]$. Rewriting the generative model with those assumptions and explicitly including parameters, we obtain equation (6). Varying the hyperparameters θ effectively leads to different generative models.

$$\mathbf{y}|\theta \sim \mathcal{N}(0, K(\mathbf{X}, \mathbf{X}; \sigma_f, \ell) + \sigma_n \mathbf{I}) \quad (6)$$

In a maximum likelihood estimation (MLE) approach, training the GPR model then consists in estimating the values of the hyperparameters θ leading to the generative model that is most in agreement with the training data. This is achieved by selecting θ that maximizes the likelihood $p(\mathbf{y}|\mathbf{X}, \theta)$. A closed-form equation for the likelihood $p(\mathbf{y}|\mathbf{X}, \theta)$ is made possible by the GP assumption. In practice, the log-likelihood $\log p(\mathbf{y}|\mathbf{X}, \theta)$ is used for numerical stability. Given training data (\mathbf{X}, \mathbf{y}) and denoting $\mathbf{K} = K(\mathbf{X}, \mathbf{X})$:

$$\log p(\mathbf{y}|\mathbf{X}, \theta) = -\frac{1}{2} \mathbf{y}^T (\mathbf{K} + \sigma_n^2 \mathbf{I})^{-1} \mathbf{y} - \frac{1}{2} \log \det (\mathbf{K} + \sigma_n^2 \mathbf{I}) - \frac{n}{2} \log 2\pi \quad (7)$$

In a Bayesian approach, hyperparameters are equipped with an prior distribution $p(\theta)$ and the full posterior distribution of the hyperparameters $p(\theta|\mathbf{y}, \mathbf{X})$ is inferred by leveraging Bayes' rule:

$$p(\theta|\mathbf{y}, \mathbf{X}) \propto p(\mathbf{y}|\mathbf{X}, \theta)p(\theta) \quad (8)$$

Predictions \mathbf{y}_* at validation locations \mathbf{X}_* can be made by recalling that the underlying process is assumed to be a GP, therefore the training and test outputs are distributed according to the following joint probability distribution:

$$\begin{bmatrix} \mathbf{y} \\ \mathbf{y}_* \end{bmatrix} \sim \mathcal{N}\left(0, \begin{bmatrix} K(\mathbf{X}, \mathbf{X}) + \sigma_n^2 \mathbf{I} & K(\mathbf{X}, \mathbf{X}_*) \\ K(\mathbf{X}_*, \mathbf{X}) & K(\mathbf{X}_*, \mathbf{X}_*) + \sigma_n^2 \mathbf{I} \end{bmatrix}\right) \quad (9)$$

The posterior predictive distribution is obtained by conditioning the joint distribution with respect to the training data. Once again, the GP assumption allows to derive this joint distribution analytically:

$$\mathbf{y}_*|\mathbf{X}_*, \mathbf{X}, \mathbf{y}, \theta \sim \mathcal{N}(\mu_*, \Sigma_*) \quad (10)$$

with:

$$\mu_* = K(\mathbf{X}_*, \mathbf{X}) (K(\mathbf{X}, \mathbf{X}) + \sigma_n^2 \mathbf{I})^{-1} \mathbf{y} \quad (11)$$

$$\Sigma_* = K(\mathbf{X}_*, \mathbf{X}_*) - K(\mathbf{X}_*, \mathbf{X}) (K(\mathbf{X}, \mathbf{X}) + \sigma_n^2 \mathbf{I})^{-1} K(\mathbf{X}, \mathbf{X}_*) \quad (12)$$

In the fully Bayesian approach to GP, the hyperparameters need to be marginalized out using their posterior distribution to make predictions:

$$p(\mathbf{y}_*|\mathbf{X}_*, \mathbf{X}, \mathbf{y}) = \int p(\mathbf{y}_*|\mathbf{X}_*, \mathbf{X}, \mathbf{y}, \theta)p(\theta|\mathbf{X}, \mathbf{y}) d\theta \quad (13)$$

2.3 Active Subspace

The active subspace (AS) method addresses challenges raised by functions of high-dimensional inputs and the resulting *curse of dimensionality*, that hinders the use of such functions in numerical activities such as uncertainty quantification, surrogate modeling, or numerical optimization. In simple terms, the method seeks directions in input space that contribute in average the most to the variation of the output. Those directions form the basis of a low-dimensional subspace of the original input space, the so-called *active subspace*. The curse of dimensionality is alleviated by substituting the active subspace to the original high-dimensional input space, obtaining a new, approximate mapping whose input space is effectively lower than the original function. AS is a general-purpose method in the sense this alternate mapping can be used to assist any of the aforementioned numerical applications.

The following paragraphs recall the major results pertaining to AS. Interested readers can find more details in [65]. In the context of the AS method, we equip the input variables \mathbf{x} of f with a probability distribution $p(\mathbf{x})$. The uncentered covariance matrix of the gradient \mathbf{C} plays a central role in the AS method:

$$\mathbf{C} = \int (\nabla_{\mathbf{x}} f)(\nabla_{\mathbf{x}} f)^T p(\mathbf{x}) d\mathbf{x} \quad (14)$$

The real symmetric matrix \mathbf{C} is then diagonalized as $\mathbf{C} = \mathbf{Q}\mathbf{\Lambda}\mathbf{Q}^T$ where $\mathbf{Q} = [\mathbf{w}_1, \dots, \mathbf{w}_d]$ is the matrix containing the normalized eigenvectors $\{\mathbf{w}_i \mid i = 1, \dots, d\}$ of \mathbf{C} and $\mathbf{\Lambda}$ is a diagonal matrix whose diagonal contains the eigenvalues $\{\lambda_i \mid i = 1, \dots, d\}$ of \mathbf{C} . We assume the eigenvalues to be sorted such that $\lambda_1 \geq \dots \geq \lambda_d \geq 0$.

The following relationship links the eigenvalues with the projections of the function's gradient onto the corresponding eigenvectors [65]. For $i = 1, \dots, d$:

$$\lambda_i = \int \left((\nabla_{\mathbf{x}} f)^T \mathbf{w}_i \right)^2 p(\mathbf{x}) d\mathbf{x} \quad (15)$$

The higher the λ_i , the greater the variations of f in the direction \mathbf{w}_i . The active subspace is defined as the subspace spanning the first $m \leq d$ directions $\{\mathbf{w}_i \mid i = 1, \dots, m\}$. In this subspace, the variations of f are in average greater than in its orthogonal complement, referred to as the *inactive subspace*.

Because they are the eigenvectors of a real symmetric matrix, the vectors $\{\mathbf{w}_i \mid i = 1, \dots, d\}$ form an orthonormal basis of the input space. We can then arrange them into two matrices:

$$\mathbf{W} = [\mathbf{w}_1, \dots, \mathbf{w}_m] \quad (16)$$

$$\mathbf{W}_i = [\mathbf{w}_{m+1}, \dots, \mathbf{w}_d] \quad (17)$$

\mathbf{W} is the $d \times m$ projection matrix onto the *active* subspace while \mathbf{W}_i is the $d \times (d - m)$ projection matrix onto the *inactive* subspace. The original mapping of interest can then be rewritten as $f(\mathbf{x}) = f(\mathbf{W}\mathbf{z} + \mathbf{W}_i\mathbf{z}_i)$ where $\mathbf{z} = \mathbf{W}^T \mathbf{x}$ is the component of the inputs in the AS and $\mathbf{z}_i = \mathbf{W}_i^T \mathbf{x}$ is the component of the inputs in the inactive subspace. Starting from this decomposition, a series of approximations can be made to obtain a practical AS-assisted surrogate modeling approach. Given the conditional probability $p(\mathbf{z}_i|\mathbf{z})$ of the inactive variables given the active variable, we start by defining the link function g as the conditional expectation of f over the inactive subspace given a position in the active subspace:

$$g(\mathbf{z}) = \mathbb{E}_{\mathbf{z}_i|\mathbf{z}} [f(\mathbf{W}\mathbf{z} + \mathbf{W}_i\mathbf{z}_i)] \quad (18)$$

By assuming that the variations of f caused by variations of input variables in the inactive subspace are substantially less than those caused by variations in the active subspace, we obtain the following approximation:

$$f(\mathbf{x}) \approx g(\mathbf{W}^T \mathbf{x}) \quad (19)$$

Since the exact integration in (19) would be either too costly or simply not possible, a Monte-Carlo approximation \hat{g} of g is used:

$$f(\mathbf{x}) \approx \hat{g}(\mathbf{W}^T \mathbf{x}) \quad (20)$$

The Monte-Carlo integration is shown to have good convergence properties in [65] since f does not by construction greatly vary in the inactive subspace. The function \hat{g} is itself approximated by a surrogate model \tilde{g} based on a limited number of model observations:

$$f(\mathbf{x}) \approx \tilde{g}(\mathbf{W}^T \mathbf{x}) \quad (21)$$

Finally, an approximation $\hat{\mathbf{W}}$ of \mathbf{W} is obtained by replacing the integral with a finite sum in the computation of the uncentered covariance matrix of the gradient shown in equation (14):

$$f(\mathbf{x}) \approx \tilde{g}(\hat{\mathbf{W}}^T \mathbf{x}) \quad (22)$$

AS-assisted surrogate modeling methods rely on equation (22) to approximate the original function f [65] by following a two-step approach. An approximation $\hat{\mathbf{W}}$ of the projection matrix \mathbf{W} onto the AS is first computed using a sample of gradient evaluations. An approximation \tilde{g} of the link function g is then constructed using traditional surrogate modeling techniques.

2.4 Gaussian Processes with Built-In Dimensionality Reduction

In the absence of gradient evaluations, it is impossible to carry out the methodology presented above to create a surrogate model that leverages the low-dimensional structure of the AS. An alternative approach proposed in [35] is to simultaneously train the approximate link function \tilde{g} and the approximate projection matrix $\hat{\mathbf{W}}$ onto the AS. The underlying predictive model combines aspects of the original AS method with Gaussian processes: the original inputs are projected onto a low-dimensional subspace that serves as the alternate, low-dimensional input space for a GP. This leads to the following model:

$$\mathbf{y}|\theta, \mathbf{W} \sim \mathcal{N}(0, K(\mathbf{XW}, \mathbf{XW}; \theta)) \quad (23)$$

This model can be broken down into two steps. An initial *projection step* where the original design matrix \mathbf{X} is projected in the AS to obtain a lower-dimensional design matrix $\mathbf{Z} = \mathbf{XW}$ followed by a *regression step* in which the lower-dimensional space is substituted to the original high-dimensional input space.

Compared to traditional GPR, this approach leads to the effective dimension reduction of GP's input space from the original d inputs to only m inputs. As a consequence, the number of GP hyperparameters is also decreased from $d + 2$ to $m + 2$. However, the projection matrix \mathbf{W} is introduced as a new model parameter that must be determined in the training process.

Following the assumptions of the AS method, the projection matrix \mathbf{W} is orthonormal. This translates into a constraint that needs to be satisfied during the process by which model parameters are selected or inferred. In an MLE approach where parameters are selected through an optimization scheme, multiple practical strategies exist for handling this constraint. In [35, 53, 49], the constraint satisfaction is ensured by restricting \mathbf{W} to the Stiefel and Grassmann manifolds using manifold optimization techniques. In [61], an orthonormalization scheme is applied to an unconstrained matrix.

2.5 Proposed Fully Bayesian Approach

Existing MLE approaches do not enable a full quantification of epistemic uncertainty due to limited model observations. After projection of the design matrix onto the AS, predictive uncertainty only originates from the assumption that the link function is modelled as a GP. However, neither the uncertainty in the GP hyperparameters nor in the projection matrix \mathbf{W} are quantified. This work introduces a fully Bayesian approach to training the model, in which full distributions for both the GP hyperparameters and the projection matrix \mathbf{W} are obtained. As a result, predictive uncertainty accounts for all uncertain model parameters.

While practical implementations of optimizations methods exist that handle parameters belonging to Riemannian manifolds, e.g. [66] used in [49], probabilistic inference packages are restricted to parameters defined in Euclidean spaces [67, 68]. Since the implementation of a robust Riemannian MCMC [55, 62] sampler is out of the scope of the present work, alternative methods were favored, that rely on a parametrization of the projection matrix \mathbf{W} using real-valued parameters.

To enforce the orthonormality constraint, the projection matrix \mathbf{W} can be interpreted as an element of the Stiefel manifold [35]. The Stiefel manifold $V_m(\mathbb{R}^d)$ is the set of ordered orthonormal m -tuples of vectors in \mathbb{R}^d . Some authors [69, 49] further restrict \mathbf{W} to the Grassmann manifold $\text{Gr}(m, d)$ of m -dimensional linear subspaces of \mathbb{R}^d , thus excluding redundant projections onto the same subspace. We remain in the Stiefel manifold in this work. In this case, the parametrization of the projection matrix by the set of parameters $\theta_{\mathbf{p}}$ is the mapping \mathcal{P} that associates a vector of k real parameters to a $d \times m$ orthonormal matrix:

$$\begin{aligned} \mathcal{P} : \mathbb{R}^k &\rightarrow V_m(\mathbb{R}^d) \\ \theta_{\mathbf{p}} &\rightarrow \mathbf{W} = \mathcal{P}(\theta_{\mathbf{p}}) \end{aligned} \quad (24)$$

The choice of \mathcal{P} is driven by the need to equip \mathbf{W} with a meaningful prior distribution while recalling that the matching distribution on the parameters $\theta_{\mathbf{p}}$ is the one that is actually implemented in the statistical inference process. Along with \mathcal{P} , the distribution of $\theta_{\mathbf{p}}$ that results in the desired distribution for \mathbf{W} is needed. The prior distribution placed on \mathbf{W} must translate the prior belief on possible AS directions: *a priori*, any set of orthonormal directions are equally probable candidates for the AS and the probability density should be spread uniformly across the Stiefel manifold. The counterpart to the uniform distribution in the Stiefel manifold is the distribution according the Haar measure [58].

Algorithm 1: \mathcal{H} : orthonormal matrix parametrization through Householder transformations

input : parameters $\theta_{\mathbf{p}} \in \mathbb{R}^k$
output : projection matrix $\mathbf{W} \in V_m(\mathbb{R}^d)$

$\mathbf{Q} \leftarrow \mathbf{I} \in \mathbb{R}^{d \times d}$
 $l \leftarrow 0$
for $i \leftarrow 1$ **to** m **do**
 $k \leftarrow l$
 $l \leftarrow k + d - i$
 $\mathbf{v} \leftarrow (\theta_{p,k}, \dots, \theta_{p,l})^T$
 $\mathbf{u} \leftarrow \frac{\mathbf{v} + \text{sgn}(v_1) \|\mathbf{v}\| \mathbf{e}_1}{\|\mathbf{v} + \text{sgn}(v_1) \|\mathbf{v}\| \|\mathbf{e}_1\|}$
 $\hat{\mathbf{H}} \leftarrow -\text{sgn}(v_1)(\mathbf{I} - 2\mathbf{u}\mathbf{u}^T)$
 $\mathbf{H} \leftarrow \begin{pmatrix} \mathbf{I} & 0 \\ 0 & \hat{\mathbf{H}} \end{pmatrix}$
 $\mathbf{Q} \leftarrow \mathbf{H}\mathbf{Q}$
end
 $\mathbf{W} \leftarrow (\mathbf{Q}_1, \dots, \mathbf{Q}_m) \in \mathbb{R}^{d \times m}$

Algorithm 2: Proposed Fully Bayesian Model

$\theta_{p,i} \sim \mathcal{N}(0, 1) \quad \forall i = 1, \dots, k$
 $\mathbf{W} = \mathcal{H}(\theta_{\mathbf{p}})$ (algorithm 1)
 $\mathbf{Z} = \mathbf{X}\mathbf{W}$
 $\log \theta_j \sim \mathcal{N}(0, 1) \quad \forall j = 1, \dots, m$
 $\mathbf{y} \sim \mathcal{N}(0, K(\mathbf{Z}, \mathbf{Z}; \theta) + \sigma_n^2 \mathbf{I})$

While the problem of parametrizing an element of the Stiefel manifold has not yet been applied in the present *supervised* dimension reduction context, solutions have been proposed for Bayesian approaches to *unsupervised* dimension reduction methods, e.g. Bayesian principal components analysis (PCA). Given rotations [60], polar expansion [59], and Householder transformations [58] have been used to that end. Among those alternatives, the parametrization through Householder transformations appears as the most practical. While other methods require a change of measure that is computationally costly due to the computation of the Jacobian determinant [58], this method directly maps independent real-valued parameters identically distributed according to the standard normal distribution to matrices that are Haar-distributed in the Stiefel manifold without needing a change of measure. The implementation details for this parametrization, adapted from [58], are presented in algorithm 1. The number k of real-valued parameters is $k = md - m(m - 1)/2$, which is larger than the actual dimension of the Stiefel manifold: $\dim(V_m(\mathbb{R}^d)) = md - m(m + 1)/2$. Doing without a change of measure comes at the cost of m additional parameters. This is not a significant penalty in practice since dimension reduction methods seek a low-dimension space such that $m \ll d$. A log-normal distribution is used as prior for the GP hyperparameters. The full proposed generative model is detailed in algorithm 2.

The joint posterior distribution $p(\theta, \theta_{\mathbf{p}} | \mathbf{X}, \mathbf{y})$ of the model parameters is obtained by conditioning the generative model shown in algorithm 2 with respect to the training data $\mathcal{D} = (\mathbf{X}, \mathbf{y})$ and performing probabilistic inference, e.g. using MCMC. The posterior distribution $p(\mathbf{W} | \mathbf{X}, \mathbf{y})$ of the projection matrix \mathbf{W} can be readily obtained by application of the Householder parametrization detailed in algorithm 1 on the MCMC samples of the marginal distribution $p(\theta_{\mathbf{p}} | \mathbf{X}, \mathbf{y})$. Instead of a point-based estimation of the AS, the proposed method therefore grants access to a full distribution. In contrast to traditional GPR (equation (13)), fully Bayesian predictions in the proposed approach require marginalizing over both the GP hyperparameters and the projection parameters:

$$p(\mathbf{y}_* | \mathbf{X}_*, \mathbf{X}, \mathbf{y}) = \iint p(\mathbf{y}_* | \mathbf{X}_*, \mathbf{X}, \mathbf{y}, \theta, \theta_{\mathbf{p}}) p(\theta, \theta_{\mathbf{p}} | \mathbf{X}, \mathbf{y}) d\theta d\theta_{\mathbf{p}} \quad (25)$$

where equation (10) is used to compute the term $p(\mathbf{y}_* | \mathbf{X}_*, \mathbf{X}, \mathbf{y}, \theta, \theta_{\mathbf{p}})$ after projecting the input design matrix \mathbf{X} onto the AS.

3 Results

A comparative study is carried out to characterize the performance of the proposed method. This section starts with a presentation of the experimental setup used for this comparative study. The next two sections present results for each group of datasets: analytical functions and datasets from science and engineering. For both groups, results on all four metrics of interest are presented and discussed.

3.1 Experimental Setup

3.1.1 Benchmark Methods

Two state-of-the-art methods are used as benchmarks. The proposed fully Bayesian method discussed in section 2.5 is referred to as Bayesian active subspace (B-AS) in the rest of this section.

MO-AS The first benchmark method was proposed in [49], which is based on the Gaussian processes with built-in dimensionality reduction methodology, proposed in [35] and discussed in section 2.4. Enhancements include: a) the use of a state-of-the-art manifold optimization library [66], and b) optimization in the Grassmann manifold instead of the Stiefel manifold. It is referred to as manifold optimization-based active subspace (MO-AS) in this section. In the same spirit as our proposed method, it aims at simultaneously identifying the orthogonal projection onto the AS and the mapping from the AS to the output space. However, it does not include any mechanism for quantifying uncertainty in the identified AS.

B-GP The second benchmark method is based on the method proposed in [70] and referred to as Bayesian Gaussian process (B-GP) in this section. In this method, a GPR model is first built on the full-dimensional input space. Instead of gathering gradient samples and using a Monte-Carlo (MC) approximation, the assumptions of the GPR model then allow a fully analytical derivation of the uncentered covariance matrix of the gradient. The AS is obtained by performing a singular value decomposition of this matrix, which therefore plays a central role in the original AS method. If the GPR model is trained in a Bayesian fashion and distributions for its hyperparameters are obtained, the uncertainty on the AS itself can be inferred using MC.

The computation of the uncentered covariance matrix of the gradient implemented in the context of this study is only semi-analytical. GP gradient evaluations are made analytically once the posterior distribution of the GP hyperparameters has been inferred, but MC is used to approximate the covariance matrix using 1000 gradient samples. This was done because an exact reproduction of the process in [70] brought excessive complexity and long runtimes. Given the high number of gradient samples used for the MC approximation, this modification is not expected to alter results. Improving on the methodology proposed in the original paper where approximate inference is used, full inference of the GP hyperparameters distribution is here carried out using MCMC.

Implementation Details The B-AS and B-GP methods were implemented using the probabilistic programming language *numpyro* [67, 71], which uses *JAX* [72] as computational backend. The MO-AS method was implemented using a version of the *pymanopt* framework [66] modified to use *JAX*. Using the same computational backend across all three methods helps in ensuring a level playing field for the comparative study such that differences in training time can be linked to the methods themselves instead of implementation specifics. For the Bayesian methods, MCMC is used for inference, leveraging the No U-Turn Sampler (NUTS) as implemented in *numpyro*. Four parallel chains are sampled, each consisting of 1000 samples from the joint posterior probability distribution on model parameters and initialized using 500 warmup samples. For MO-AS, 500 restarts of the manifold optimization algorithm are used, as in [49]. The implementation of the three models used to produce the results presented in this paper are available online².

3.1.2 Benchmark Datasets

The comparison of the proposed method’s performance with benchmark method is drawn based on datasets generated using analytical functions and on datasets originating from science and engineering. While analytical datasets enable fast data generation and freedom to hand-pick functional features, real-life datasets allow assessment of the proposed method’s capabilities in a more realistic setting.

²https://github.com/rhgautier/Bayesian_dimension_reduction

		Sample Size	Input Space Dimension	Active Subspace Dimension	Reference
Analytical Quadratic Functions (QF)	QF 10/1	1000	10	1	–
	QF 10/2	1000	10	2	–
	QF 25/1	1000	25	1	–
	QF 25/2	1000	25	2	–
	QF 50/1	1000	50	1	–
	QF 50/2	1000	50	2	–
	QF 100/1	1000	100	1	–
	QF 100/2	1000	100	2	–
Science and Engineering	NACA0012 (lift)	1756	18	1	[65]
	HIV at $t = 3400$	1000	27	1	[73]
	ONERA M6 (lift)	297	50	1	[74]
	Elliptic PDE	1000	100	1	[44]

Table 1: Summary of benchmark datasets

Analytical functions are chosen to be quadratic functions featuring an AS by construction. As before, d and m are respectively the dimensions of the input space and active subspace. The quadratic functions f are defined as:

$$\mathbf{z} = \mathbf{W}^T \mathbf{x} \quad (26)$$

$$f(\mathbf{x}) = \mathbf{z}^T \mathbf{A} \mathbf{z} + \mathbf{b} \mathbf{z} + c + \epsilon \quad (27)$$

where \mathbf{x} and \mathbf{z} are respectively the input vector and the vector of projected coordinates in the AS. \mathbf{W} is the $d \times m$ projection matrix onto the AS. $\mathbf{A} \in \mathbb{R}^{m \times m}$, $\mathbf{b} \in \mathbb{R}^m$, and $c \in \mathbb{R}$ are parameters of the quadratic mappings. Given d and m , their coefficients are sampled from standard normal distributions to obtain randomly generated mappings. Since the domains of the quadratic mappings are restricted to their respective AS by construction, an additive centered Gaussian noise ϵ of standard deviation 5×10^{-2} is added to simulate the variation of the response due to variations of the inputs in the inactive subspace. In the context of the present study, eight quadratic functions were generated, that combine an input space dimension d of 10, 25, 50, or 100 with an AS dimension of 1 or 2.

Four datasets originating from scientific and engineering applications are also used to assess the proposed method. These datasets were previously used in AS-related studies and include gradient evaluations in addition to input-output pairs. Gradient evaluations are used to estimate the actual AS using the original AS method, which is needed to assess the ability of the proposed method to uncover the AS. Those datasets cover a wide range of input space dimensions: the NACA 0012 [65], HIV [73], ONERA-M6 [74], and Elliptic PDE [44] datasets respectively have 18, 27, 50, and 100 input dimensions. Based on previous studies, all of these datasets are known to have a one-dimensional AS.

3.1.3 Benchmark Metrics

The comparative study focuses on the four following aspects: a) capability to uncover the AS, b) deterministic predictive capability, c) probabilistic predictive capability, and d) computational cost. To each aspect corresponds a numerical metric enabling the quantitative comparison of the proposed method with both benchmark methods: a) subspace angles, b) root-mean-square error, c) posterior normalized validation log-likelihood, and d) training time. These metrics are briefly defined in the following paragraphs.

First Subspace Angle Successful recovery of the AS can be assessed by estimating the subspace angles between the low-dimensional subspace found during training and the actual AS [70]. Subspace angles are defined in [75]. The reference AS is computed using the original AS method [65] presented in section 2.3. This is possible because all test datasets include gradient evaluations. For each dataset, all available gradient samples are used to estimate the reference AS in an effort to maximize the quality of the MC estimator $\sum_{i=0}^n \nabla f(\mathbf{x}_i) \nabla f(\mathbf{x}_i)^T$. By definition of the angles between subspaces, the first subspace angle is greater than the following angles and is therefore an upper bound for all subspace angles. For this reason and because using a single numerical value eases comparison between methods, the first subspace angle will be used as metric.

Root-Mean-Square Error The deterministic predictive capability refers to the quality of point predictions made by the model. For fully Bayesian methods, the median of the posterior predictive distribution at a previously unobserved site \mathbf{x}^* is used as the point estimate $\hat{f}(\mathbf{x}^*)$. Given n test points $\{\mathbf{x}_1^*, \dots, \mathbf{x}_n^*\}$ distributed according to the distribution

$p(\mathbf{x})$, the root-mean-square error (RMSE) metric is used to quantify deterministic predictive capability is defined as:

$$\text{RMSE} = \sqrt{\frac{1}{n} \sum_{i=1}^n \left(f(\mathbf{x}_i^*) - \hat{f}(\mathbf{x}_i^*) \right)^2} \quad (28)$$

Validation Normalized Posterior Log-Likelihood The probabilistic predictive capability refers to the quality of the probability distributions outputted by the model. Because the computer models under consideration are deterministic mappings, the likelihood of observing the actual point output under the posterior predictive can be used as a metric.

We consider every validation sample (\mathbf{x}_i^*, y_i^*) for $i = 1, \dots, n$ independently. The posterior predictive distribution was recalled in equation (10). With μ_i^* and σ_i^{*2} respectively computed using equations (11) and (12), we obtain the following expression:

$$\log p(y_i^* | \mathbf{x}_i^*, \mathbf{X}, \mathbf{y}) = -\frac{1}{2} \frac{(y_i^* - \mu_i^*)^2}{\sigma_i^{*2}} - \log \sigma_i^* - \frac{\gamma}{2} \log 2\pi \quad (29)$$

where $\gamma = m$ for the MO-AS and B-AS methods and $\gamma = d$ for the B-AS method. For fully Bayesian methods, marginalization with respect to the hyperparameters is necessary:

$$\log p(y_i^* | \mathbf{x}_i^*, \mathbf{X}, \mathbf{y}) = \log \left(\iint p(y_i^* | \mathbf{x}_i^*, \mathbf{X}, \mathbf{y}, \theta, \theta_{\mathbf{p}}) p(\theta, \theta_{\mathbf{p}} | \mathbf{X}, \mathbf{y}) d\theta_{\mathbf{p}} d\theta \right) \quad (30)$$

Computation of the double integral in equation (30) relies on a Monte-Carlo approximation that uses the samples from the joint posterior distribution $p(\theta, \theta_{\mathbf{p}} | \mathbf{X}, \mathbf{y})$ obtained through MCMC. In order to account for different number of validation samples across cases, we normalize as follows:

$$\text{VNPLL} = \frac{1}{n} \sum_{i=1}^n \log p(y_i^* | \mathbf{x}_i^*, \mathbf{X}, \mathbf{y}) \quad (31)$$

Training Time Finally, the training time is measured as the wall-clock time elapsed between the start and the end of the model training.

3.2 Quadratic Functions

3.2.1 Active Subspace Recovery

Figure 1 depicts the evolution of the first subspace angle as a function of the number of samples used to train the model. A low subspace angle indicates that the inferred and true active subspaces are nearly aligned, corresponding to a successful recovery of the AS. Across all models and datasets, trends seem to indicate that a minimum number of training samples is required to successfully recover the AS, which is indicated by the drop of the subspace angle metric.

We note that, in the case of both B-GP and B-AS, the observed variability originates from both the repetition using different training samples and the uncertainty in the AS captured by the Bayesian approaches. On the other hand, point estimations of the AS are made for MO-AS, and variability is therefore only the results of training repetitions. This explains why the subspace angle distributions have wider spread for the Bayesian approaches than for the optimization-based approach.

For all eight benchmark quadratic functions, we observe that B-GP consistently exhibits worse AS recovery capabilities than the other two methods. The performance of B-GP also decreases with the number of input dimensions. While the drop in first subspace angle, characteristic of successful AS recovery, is indeed visible within the range of training set sizes under study when $d = 10$ and $d = 25$, no such drop is visible when $d = 50$ and $d = 100$. Actively seeking the AS by adapting the form of the predictive model to incorporate a projection onto a lower-dimensional subspace therefore appears to drastically improve the ability of surrogate-based methods to detect the AS when a limited number of training samples is available.

Both the B-AS and MO-AS have similar AS recovery capabilities. As noted earlier, the distributions for the B-AS method have wider spread due to the Bayesian nature of the method: instead of only seeking the most likely AS, the proposed B-AS gives access to the full posterior distribution of the AS. Directions that are less likely given the model observations are therefore retained and given a smaller weight. We will see that it enables better quantification of the epistemic uncertainty. We also note the skewness of some of those distributions, such as for $d = 25$, $m = 1$, and 50 or 75 training samples: while the distribution almost spans the complete interval of subspace angle values, most of its weight is concentrated on small angle values. Both methods consistently enable the detection of the AS a number of training samples smaller than five times the number of dimensions for 25- to 100-dimensional quadratic functions.

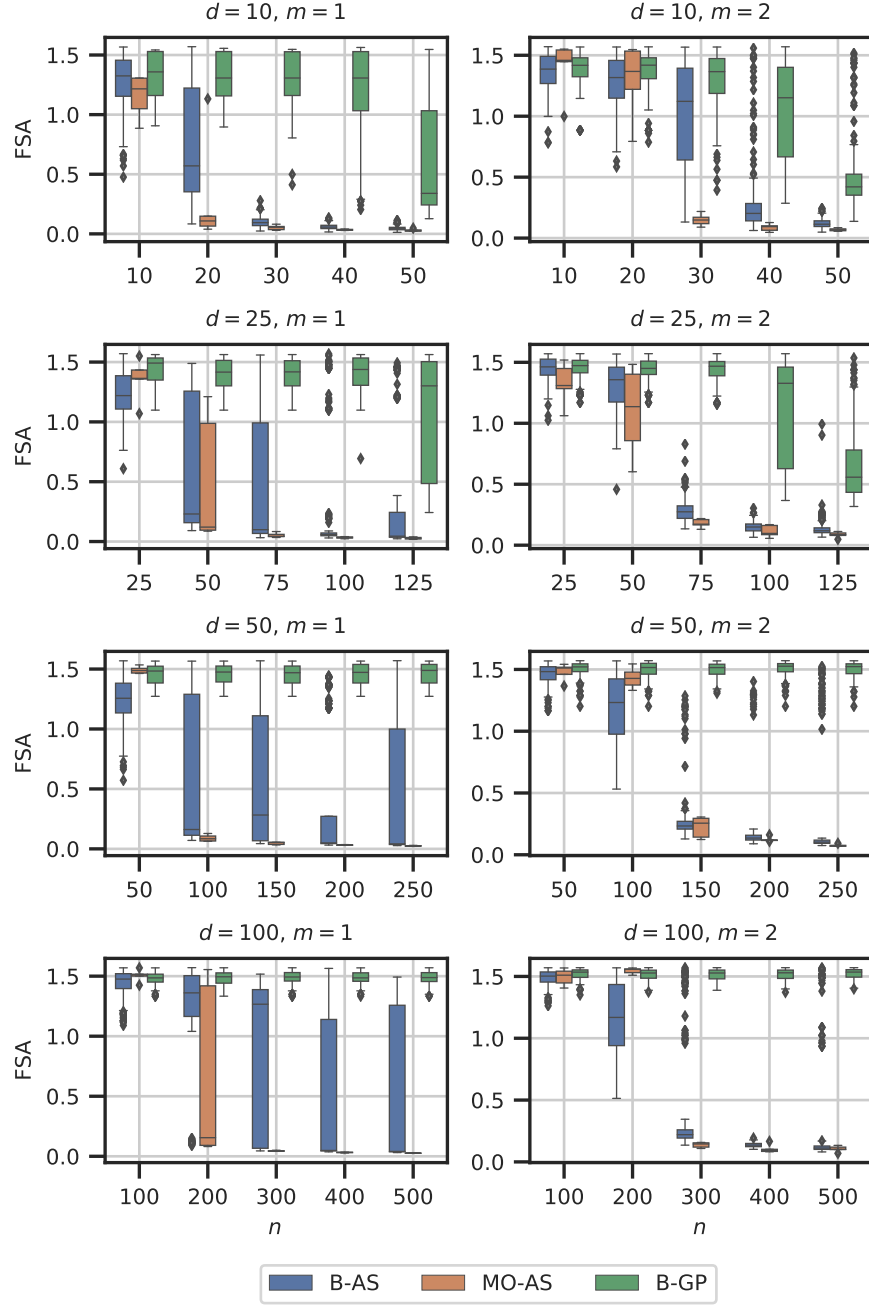


Figure 1: Evolution of the first subspace angle (FSA) between the predicted and actual active subspaces for training sets varying in size n from one to five times the number of input dimensions for quadratic function datasets. Plots are organized by increasing input dimension d from top to bottom and by increasing AS dimension m from left to right.

3.2.2 Deterministic Predictive Capability

Figure 2 depicts the evolution of the RMSE as a function of the number of samples used to train the predictive model. For both Bayesian approaches, the median is used for point-based prediction.

The deterministic predictive capability of B-GP for high-dimensional input spaces is consistent with its poor ability to detect the AS: it nearly always scores worse than both other methods. The relative drop in performance with an increasing number of input dimensions first observed with the first subspace angle is here confirmed: the deterministic predictions of B-GP do not improve over the studied range of training samples neither for $d = 50$ nor for $d = 100$.

The comparison of the B-AS and MO-AS methods indicates that both methods perform equally well for a number of training samples ranging from three to five times the number of input space dimensions. For very small training sets however, the MO-AS invariably displays much higher RMSE values than the other two methods. This is consistent with the expected superiority of Bayesian methods when few model observations are available. In the light of those results, the proposed B-AS approach therefore appears to improve upon the MO-AS approach: it reaches the same performance when a relatively high number of training samples are available while increasing performance when only few model observations are available.

3.2.3 Probabilistic Predictive Capability

Figure 3 shows the evolution of the validation normalized posterior log-likelihood as the number of training samples is increased. This metric reveals the quality of the probabilistic prediction: the higher the posterior log-likelihood, the most likely it is to observe the actual responses of the validation dataset under the posterior of the predictive model.

As expected, Both Bayesian methods consistently score better than MO-AS with respect to this metric. Except for the case $d = 100, m = 1$, MO-AS always displays poorer probabilistic predictive capabilities than both other methods. This can be explained by the fact that uncertainty in the MO-AS model is only partially captured: while the GP effectively captures part of the uncertainty, neither the uncertainty in the GP hyperparameters nor in the projection matrix parameters is quantified. Except for the case $d = 100, m = 1$ where a large variability of the predictive capability across training sets is observed among smaller training sets, the proposed B-AS generally leads to posterior predictive distributions that are in greater agreement with actual validation data. B-GP displays a performance similar to B-AS for small training sets but is overtaken by B-AS for larger training sets.

3.2.4 Training Time

Figure 4 depicts the evolution of the time required to train all three types of models for the different quadratic functions under study. Training time always increases with the number of training samples. This is expected as the cost of computing the inverse of the sample covariance matrix during the GP likelihood computation increases as the matrix size increases. For $d = 50$ and $d = 100$, a linear trend in log-scale is clearly visible, that corresponds to a power-law scaling in linear scale. Such a behavior is expected for B-GP, for which the $\mathcal{O}(n^3)$ scaling is well-known, where n is the number of training samples.

The B-GP models are consistently faster to train than both projection-based methods. This is expected since those methods require additional computations during the models' likelihood evaluation and increase the number of parameters to be inferred or optimized without affecting the size of the sample covariance matrix, which is the bottleneck of GP training.

While the proposed B-AS model trains faster than the MO-AS model for low input space dimensions and low number of training samples, its training time becomes larger when dimension and training samples increase. This may be explained by considering the differences between the two methods. On the one hand, in MO-AS, the number of restarts of the gradient-based optimization is fixed but the number of steps during one optimization run (and therefore the number of likelihood evaluations) may vary because a dynamic stopping criterion is used to terminate optimization. On the other hand, in B-AS, the MCMC chain length is fixed but the size of the leapfrog steps of the No-U-Turn Sampler (NUTS) sampler are adaptively chosen during warmup based on the shape of the likelihood function. In practice, we observed greater variability in the MCMC step size than we did in the number of optimization steps. As the number of input dimensions increases and the likelihood function becomes more challenging to sample, the step size chosen by the NUTS algorithm decreases, thus leading to more HMC leapfrog steps and increased total sampling times.

3.3 Science and Engineering Datasets

This section mirrors the preceding section by presenting results for all four metrics of interest, this time on the benchmark science and engineering datasets. While the quadratic functions may be representative of simple functions encountered

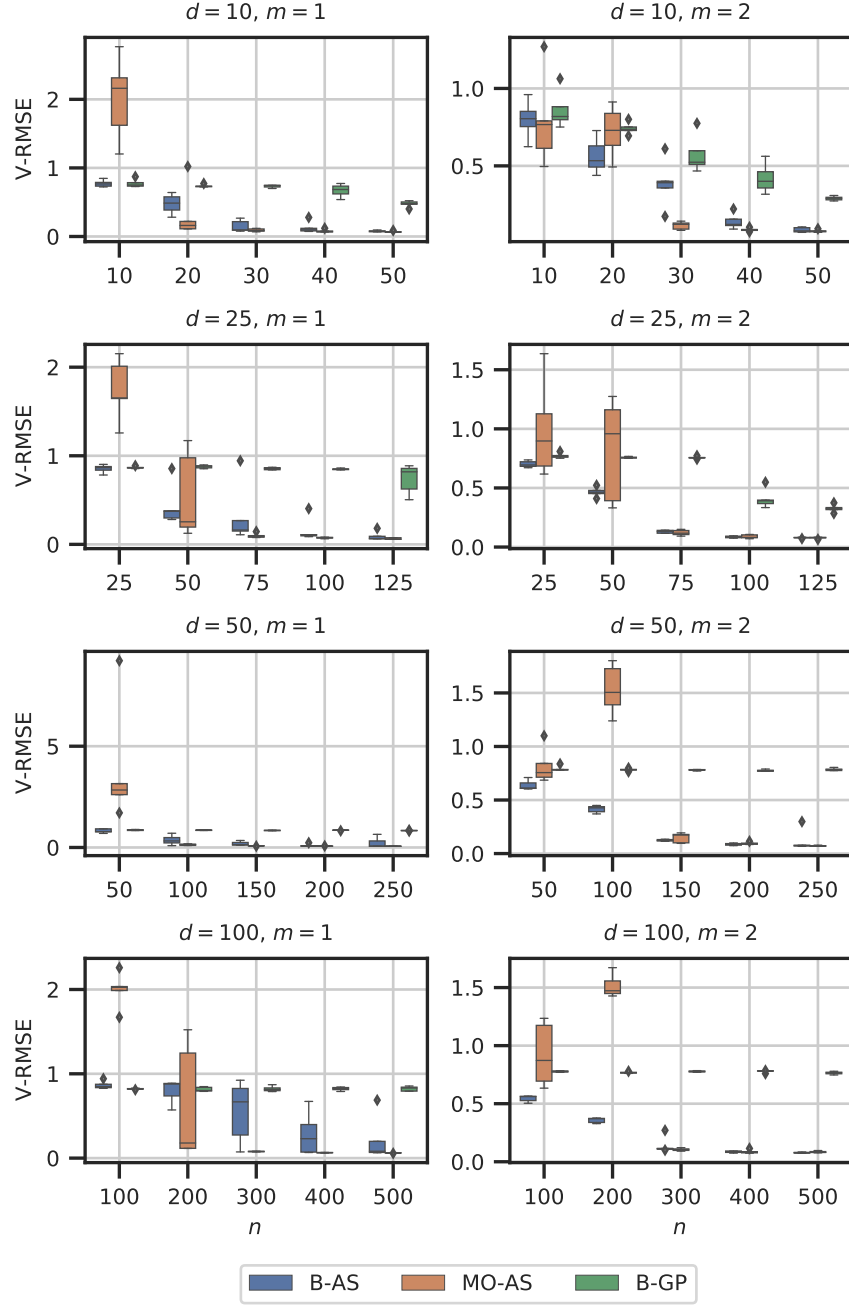


Figure 2: Evolution of the validation root-mean-square error (RMSE) for training sets varying in size n from one to five times the number of input dimensions for quadratic function datasets. Plots are organized by increasing input dimension d from top to bottom and by increasing AS dimension m from left to right.

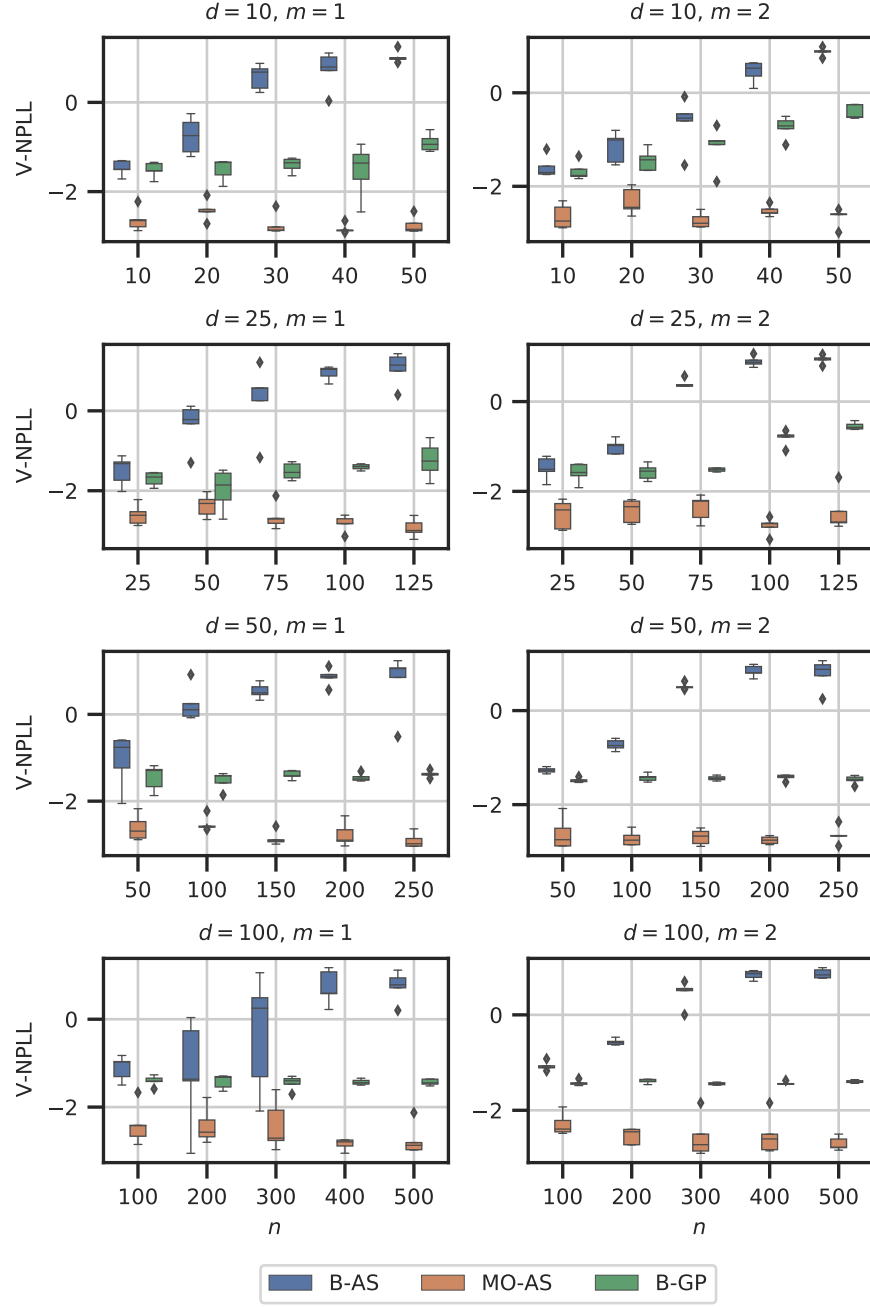


Figure 3: Evolution of the validation normalized posterior log-likelihood (V-NPLL) for training sets varying in size n from one to five times the number of input dimensions for quadratic function datasets. Plots are organized by increasing input dimension d from top to bottom and by increasing AS dimension m from left to right.

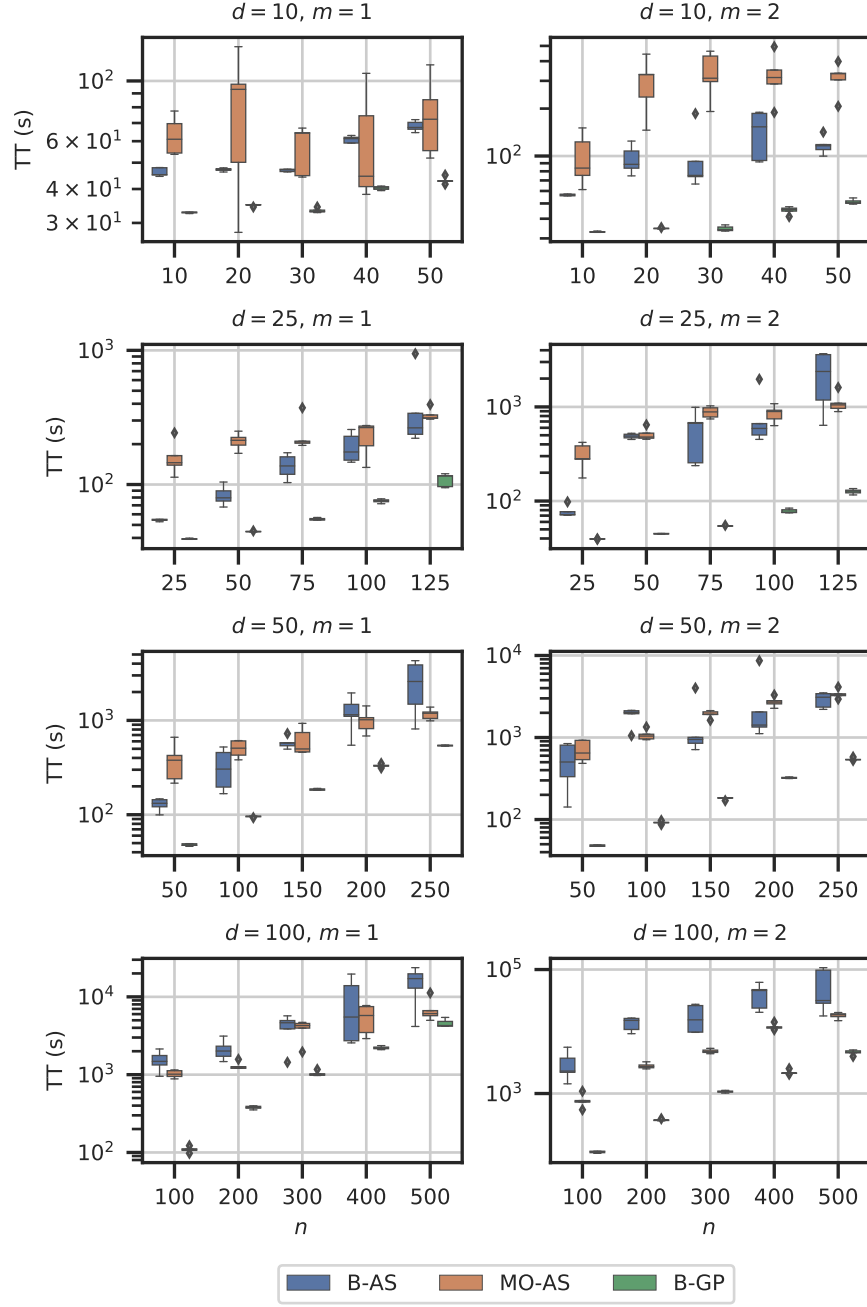


Figure 4: Evolution of the training time (TT) for training sets varying in size n from one to five times the number of input dimensions for quadratic function datasets. Plots are organized by increasing input dimension d from top to bottom and by increasing AS dimension m from left to right.

in practical engineering applications, these datasets were generated using actual analyses encountered in scientific or engineering practice.

3.3.1 Active Subspace Recovery

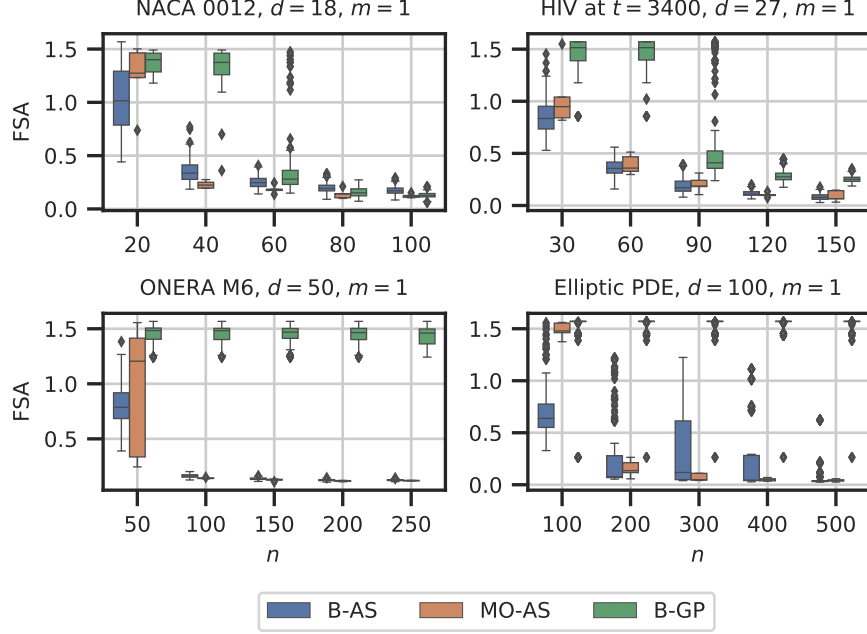


Figure 5: Evolution of the first subspace angle (FSA) between the predicted and actual active subspaces for training sets varying in size n from one to five times the number of input dimensions for all four science and engineering datasets.

Figure 5 presents the AS recovery results obtained for science and engineering datasets. Trends are similar to those encountered for the analytical functions. For the NACA 0012 dataset, which is relatively low-dimensional, the lag of B-GP is clearly visible: while both B-AS and MO-AS have started converging towards the right AS as soon as $n = 40$, B-GP still struggles at identifying the right AS, as indicated by the large values of first subspace angle. A similar behavior can be observed for the 27-dimensional HIV dataset. For both the higher-dimensional ONERA M6 and Elliptic PDE datasets, B-GP does not enable the identification of the AS within the interval of training set sizes under study.

B-AS and MO-AS still exhibit similar performance, both managing to consistently find a satisfactory approximation to the AS when the number of training samples is smaller than five times the number of inputs. B-AS still exhibits wider spread of its distributions due to the fact that variability not only originates from repetition over different training sets but also from the method’s inherent quantification of uncertainty.

3.3.2 Deterministic Predictive Capability

Figure 6 shows the evolution of the RMSE as a function of the number of training samples for the science and engineering datasets. It confirms the correlation, already observed with quadratic functions, between the ability to identify the AS and the predictive performance. For the NACA 0012 and HIV datasets, the drop in RMSE of B-GP corresponds to the drop in subspace angle observed in figure 5. For the ONERA M6 and Elliptic PDE datasets, no drop in RMSE is observed within the range of training set sizes under study, which corresponds to the inability of the method to identify the AS.

On the contrary, both projection-based methods lead to good deterministic predictive performance within the domain of study. We observe that RMSE values converge to small but non-zero values, which is an expected behavior. The model obtained by projecting the original input variables onto a lower-dimensional subspace does not account for variations of the response due to variations of the input variables in the orthogonal complement of the AS (the inactive subspace). Once the model has converged, in the sense that no improvements in predictive accuracy are observed when increasing the number of training samples, the remaining RMSE therefore corresponds to the error introduced by those

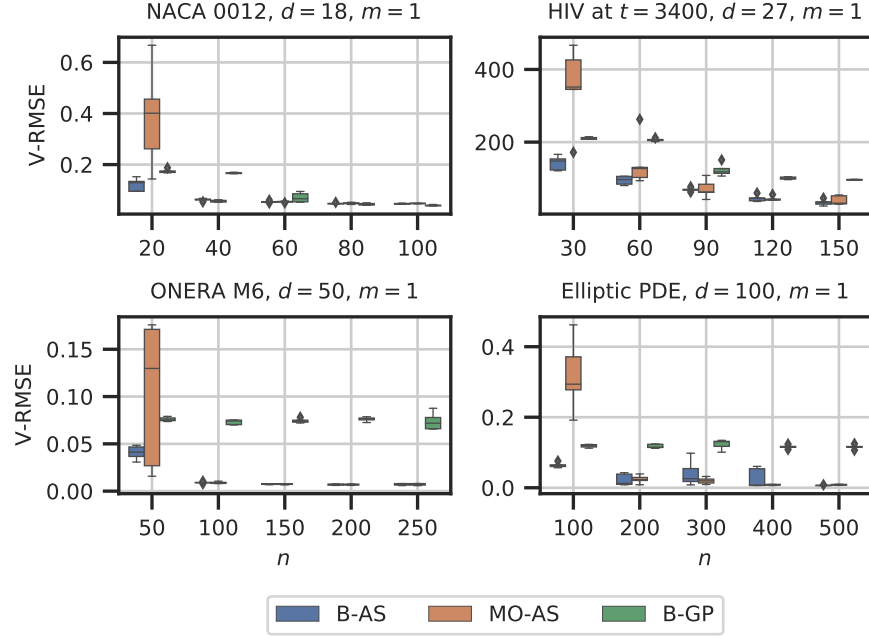


Figure 6: Evolution of the validation root-mean-square error (RMSE) for training sets varying in size n from one to five times the number of input dimensions for all four science and engineering datasets.

unaccounted-for variations. This illustrates the trade-off introduced by dimensionality reduction of the input space; it comes at the cost of introducing noise.

3.3.3 Probabilistic Predictive Capability

Figure 7 depicts the evolution of the validation normalized posterior log-likelihood for different numbers of training samples. The graph corresponding to the HIV dataset has been truncated to improve readability. For completeness, all numerical values have been included in table 2 located in Appendix A. As opposed to the results shown in 3 that were mostly consistent across different numbers of input space and active subspace dimensions, the corresponding results for science and engineering datasets seem to be highly problem-dependent.

For the relatively low-dimensional NACA0012 dataset, MO-AS displays the poorest probabilistic predictive capabilities. B-AS exhibits better performance than B-GP for small training sets, but is slightly outperformed by B-GP for larger training sets. This is an illustration of the trade-off occurring when reducing the dimensionality of the inputs. While B-GP operates on the full input space, the proposed method always operates on one of its low-dimensional subspaces. As a result, as the number of training samples increases, B-GP can start capturing variability in the response due to variations of the inputs in the inactive subspace while B-AS is limited to capturing variations of the response due to variations of the inputs in the active subspace only, and variations in the inactive subspace are captured as noise.

For the 27-dimensional HIV dataset, the proposed method behaves badly for intermediate-sized dataset and otherwise better than both other methods. Except for intermediate-sized datasets where B-AS yields particularly poor performance, MO-AS performs worse than both other methods.

The performance of the proposed B-AS method significantly improves for the two highest-dimensional datasets, ONERA M6 and Elliptic PDE, with consistently higher predictive log-likelihoods than both other methods across all training set sizes.

3.3.4 Training Time

Figure 8 shows the evolution of the training time as a function of the number of training samples. B-GP models are consistently faster to train, as fewer model parameters need to be identified compared to projection-based methods. On those four datasets, the training time of B-AS is smaller or on the same order as MO-AS, even in the case of the Elliptic

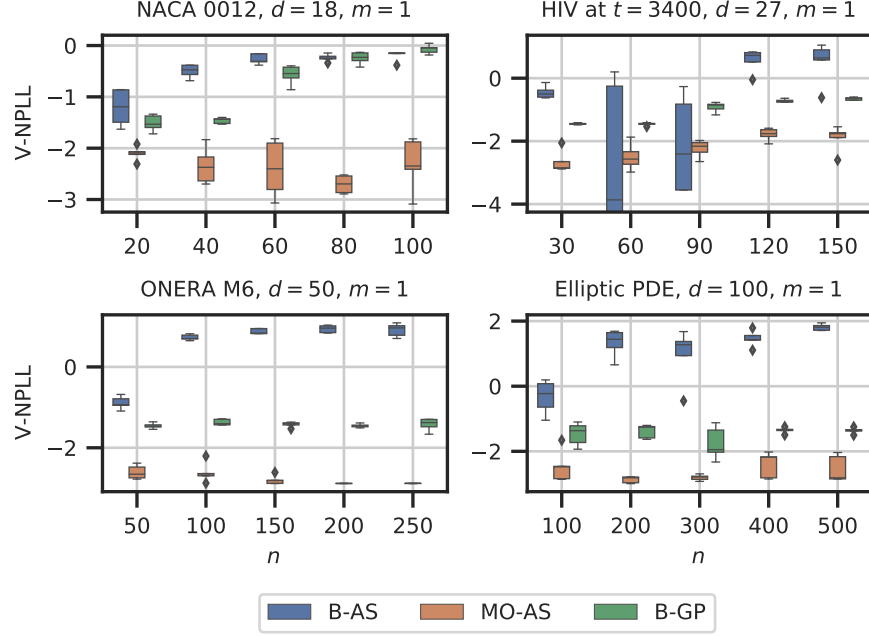


Figure 7: Evolution of the validation normalized posterior log-likelihood (V-NPLL) for training sets varying in size n from one to five times the number of input dimensions for all four science and engineering datasets.

PDE featuring a 100-dimensional input space. Beyond the expected scaling with the number of training samples and the number of inference parameters, training time appears to be highly dependent on the problem-at-hand.

4 Conclusion

The proposed B-AS method was designed to assist the creation of surrogate models of computationally expensive analyses with high-dimensional input spaces and for which access to gradients is not available. It enriches the family of projection-based methods for supervised dimension reduction with a gradient-free and fully Bayesian alternative. This work offered a comparative study of the proposed method with two other state-of-the-art methods, MO-AS and B-GP, that focused on four aspects: recovery of the active subspace, deterministic prediction accuracy, probabilistic prediction accuracy, and training time.

The study was carried out on eight analytical functions (25 to 100 inputs) and four science and engineering datasets (18 to 100 inputs) and showed the proposed method to be superior to previously introduced methods mainly due to its improved probabilistic predictive ability. Where optimization-based methods confidently make wrong predictions, the proposed method adequately estimates the uncertainty in its predictions thanks to the fully Bayesian approach. The explicit incorporation of a projection onto a lower-dimensional subspace within the form of the surrogate model was shown to ease the identification of the AS and in turn to improve the predictive capabilities of the resulting surrogate model, as opposed to the surrogate-based approaches to AS, such that B-GP, that aim at first constructing a full-dimensional surrogate model and then using it to find the AS.

While the dimension of the AS was assumed to be known throughout the present study, this is not the case in practice when being confronted to a new dataset. Existing methods to assess the AS dimension have been proposed, notably alongside the two benchmark methods used in this study. In [35], the authors propose to successively train the model assuming different AS dimensions and select the dimension based on the Bayesian information criterion (BIC). This method may be deemed unsatisfactory as it requires multiple costly training runs to obtain a single model. In [70], the original AS methodology for selecting the number of active dimensions can be carried out since a surrogate model in the full-dimensional input space is built. However, as shown in this study, significantly more samples are required to obtain a good model in the full-dimensional input space compared to methods explicitly incorporating the projection onto a low-dimensional subspace. A gradient-free method for determining the AS dimension when few model observations are available remains an open problem and will be the subject of future work.

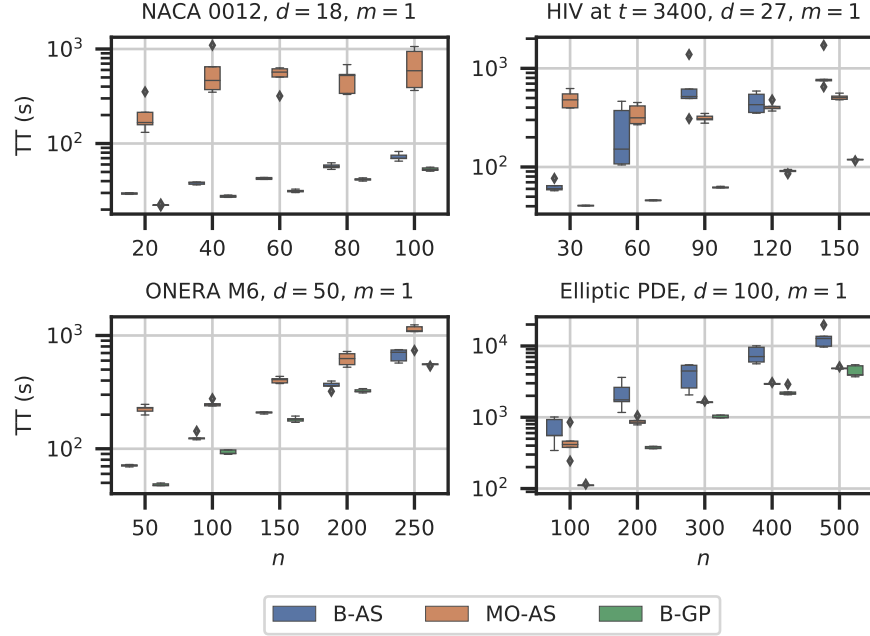


Figure 8: Evolution of the training time (TT) for training sets varying in size n from one to five times the number of input dimensions for all four science and engineering datasets.

Resorting to a surrogate modeling technique such as the one proposed in this study, that incurs a significant computational cost in addition to the cost of model evaluations, is justified for analyses whose computational cost is itself high. Given that realistic computational budgets are limited, high computational cost mechanically results in a small number of model observations. Adaptive sampling methods aim at intelligently selecting those few model observations such that the accuracy of the resulting surrogate model is maximized using predictive uncertainty. An accurate quantification of predictive uncertainty for relatively small training sets is crucial in that process, as adaptive sampling is carried out when only a limited number of model evaluations are available. The proposed method therefore appears as a viable candidate for surrogate-based adaptive sampling, as it exhibits comparable training times and often better probabilistic predictive capabilities than state-of-the-art methods. The application of the proposed method within an adaptive sampling scheme tailored to functions with high-dimensional inputs will therefore be another avenue for future work.

References

- [1] Jeremy Oakley. Estimating percentiles of uncertain computer code outputs. *Journal of the Royal Statistical Society: Series C (Applied Statistics)*, 53(1):83–93, 2004.
- [2] Nancy Flournoy. A clinical experiment in bone marrow transplantation: Estimating a percentage point of a quantal response curve. In *case studies in Bayesian Statistics*, pages 324–336. Springer, 1993.
- [3] Matthias Schonlau. *Computer Experiments and Global Optimization*. PhD thesis, University of Waterloo, 1997.
- [4] Jerome Sacks, William J Welch, Toby J Mitchell, and Henry P Wynn. Design and analysis of computer experiments. *Statistical science*, pages 409–423, 1989.
- [5] Peter Benner and Heike Faßbender. Model Order Reduction: Techniques and Tools. In *Encyclopedia of Systems and Control*, pages 1–10. Springer London, London, 2013.
- [6] I T Jolliffe. Principal Component Analysis. Encyclopedia of Statistics in Behavioral Science. In *Encyclopedia of Statistics in Behavioral Science*, page 518. John Wiley & Sons, Ltd, 2005.
- [7] Yin hao Zhu and Nicholas Zabaras. Bayesian deep convolutional encoder–decoder networks for surrogate modeling and uncertainty quantification. *Journal of Computational Physics*, 366:415–447, 2018.
- [8] Felix Dietrich, Florian Künzner, Tobias Neckel, Gerta Köster, and Hans Joachim Bungartz. Fast and flexible uncertainty quantification through a data-driven surrogate model. *International Journal for Uncertainty Quantification*, 8(2):175–192, 2018.

- [9] Christos Lataniotis, Stefano Marelli, and Bruno Sudret. Extending classical surrogate modeling to high dimensions through supervised dimensionality reduction: A data-driven approach. *International Journal for Uncertainty Quantification*, 10(1):55–82, 2020.
- [10] Khachik Sargsyan, Cosmin Safta, Habib N. Najm, Bert J. Deusschere, Daniel Ricciuto, and Peter Thornton. Dimensionality reduction for complex models via Bayesian compressive sensing. *International Journal for Uncertainty Quantification*, 4(1):63–93, 2014.
- [11] Martin Kubicek, Edmondo Minisci, and Marco Cisternino. High dimensional sensitivity analysis using surrogate modeling and high dimensional model representation. *International Journal for Uncertainty Quantification*, 5(5):393–414, 2015.
- [12] Songqing Shan and G. Gary Wang. Survey of modeling and optimization strategies to solve high-dimensional design problems with computationally-expensive black-box functions. *Structural and Multidisciplinary Optimization*, 41(2):219–241, 2010.
- [13] Sandra Keiper. Approximation of generalized ridge functions in high dimensions. *Journal of Approximation Theory*, 245:101–129, 2019.
- [14] Benjamin Doerr and Sebastian Mayer. The recovery of ridge functions on the hypercube suffers from the curse of dimensionality. *arXiv preprint arXiv:1903.10223*, 3 2019.
- [15] Dino Oglic. *Constructive Approximation and Learning By Greedy Algorithms*. PhD thesis, Universit{a}ts-und Landesbibliothek Bonn, 2018.
- [16] Andrew Glaws and Paul G. Constantine. A Lanczos-Stieltjes method for one-dimensional ridge function approximation and integration. *arXiv preprint arXiv:1808.02095*, 2018.
- [17] Anton Kolleck. *On Some Aspects of Recovery of Sparse Signals in High Dimensions from Nonlinear Measurements using Compressed Sensing*. PhD thesis, Technischen Universität Berlin, 2017.
- [18] Allan Pinkus. *Ridge functions*, volume 205. Cambridge University Press, 2015.
- [19] RA DeVore and GG Lorentz. *Constructive approximation*. Springer Science & Business Media, 1993.
- [20] Hemant Tyagi and Volkan Cevher. Learning ridge functions with randomized sampling in high dimensions. In *ICASSP, IEEE International Conference on Acoustics, Speech and Signal Processing - Proceedings*, pages 2025–2028. IEEE, 2012.
- [21] Massimo Fornasier, Karin Schnass, and Jan Vybiral. Learning Functions of Few Arbitrary Linear Parameters in High Dimensions. *Foundations of Computational Mathematics*, 12(2):229–262, 4 2012.
- [22] Albert Cohen, Ingrid Daubechies, Ronald DeVore, Gerard Kerkyacharian, and Dominique Picard. Capturing Ridge Functions in High Dimensions from Point Queries. *Constructive Approximation*, 35(2):225–243, 4 2012.
- [23] Karin Schnass and Jan Vybiral. Compressed learning of high-dimensional sparse functions. In *ICASSP, IEEE International Conference on Acoustics, Speech and Signal Processing - Proceedings*, pages 3924–3927. IEEE, 2011.
- [24] Bing Li. *Sufficient Dimension Reduction: Methods and Applications With R*. Chapman and Hall/CRC, 2018.
- [25] Christopher J.C. Burges. Dimension reduction: A guided tour. *Foundations and Trends in Machine Learning*, 2(4):275–365, 8 2009.
- [26] Kenji Fukumizu, Francis R. Bach, and Michael I. Jordan. Kernel dimension reduction in regression. *Annals of Statistics*, 37(4):1871–1905, 8 2009.
- [27] Kofi P. Adraghi and R. Dennis Cook. Sufficient dimension reduction and prediction in regression. *Philosophical Transactions of the Royal Society A: Mathematical, Physical and Engineering Sciences*, 367(1906):4385–4405, 11 2009.
- [28] Bing Li and Shaoli Wang. On directional regression for dimension reduction. *Journal of the American Statistical Association*, 102(479):997–1008, 9 2007.
- [29] Eduardo Bayro Corrochano, Tijn De Bie, Nello Cristianini, and Roman Rosipal. Eigenproblems in Pattern Recognition. *Handbook of Geometric Computing*, 10:129–167, 2005.
- [30] Roman Rosipal and Nicole Krämer. Overview and recent advances in partial least squares. *Lecture Notes in Computer Science (including subseries Lecture Notes in Artificial Intelligence and Lecture Notes in Bioinformatics)*, 3940 LNCS:34–51, 2006.
- [31] Roman Rosipal. Nonlinear partial least squares: An overview. *Chemoinformatics and Advanced Machine Learning Perspectives: Complex Computational Methods and Collaborative Techniques*, pages 169–189, 2010.

- [32] Timothy James Cole. Can partial least squares regression separate the effects of body size and growth on later blood pressure?: Partial least squares regression. *Epidemiology*, 21(4):449–451, 2010.
- [33] Shipeng Yu, Kai Yu, Volker Tresp, Hans Peter Kriegel, and Mingrui Wu. Supervised probabilistic principal component analysis. In *Proceedings of the ACM SIGKDD International Conference on Knowledge Discovery and Data Mining*, volume 2006 of *KDD '06*, pages 464–473, New York, NY, USA, 2006. ACM.
- [34] Guoqing Chao, Yuan Luo, and Weiping Ding. Recent Advances in Supervised Dimension Reduction: A Survey. *Machine Learning and Knowledge Extraction*, 1(1):341–358, 1 2019.
- [35] Rohit Tripathy, Ilias Bilonis, and Marcial Gonzalez. Gaussian processes with built-in dimensionality reduction: Applications to high-dimensional uncertainty propagation. *Journal of Computational Physics*, 321:191–223, 2016.
- [36] P. Tsilifis and R. G. Ghanem. Bayesian adaptation of chaos representations using variational inference and sampling on geodesics. *Proceedings of the Royal Society A: Mathematical, Physical and Engineering Sciences*, 474(2217), 9 2018.
- [37] Ronald DeVore, Guergana Petrova, and Przemyslaw Wojtaszczyk. Approximation of Functions of Few Variables in High Dimensions. *Constructive Approximation*, 33(1):125–143, 2011.
- [38] Yanyuan Ma and Liping Zhu. A review on dimension reduction. *International Statistical Review*, 81(1):134–150, 2013.
- [39] Peng Chen and Omar Ghattas. Hessian-based sampling for high-dimensional model reduction. *International Journal for Uncertainty Quantification*, 9(2):103–121, 2019.
- [40] Isabelle Guyon, Steve Gunn, Masoud Nikraves, and Lofti A Zadeh. *Feature extraction: foundations and applications*, volume 207. Springer, 2008.
- [41] Paul G. Constantine, Eric Dow, and Qiqi Wang. Active subspace methods in theory and practice: Applications to kriging surfaces. *SIAM Journal on Scientific Computing*, 36(4):A1500–A1524, 2014.
- [42] M. Stoyanov and C. G. Webster. A gradient-based sampling approach for dimension reduction of partial differential equations with stochastic coefficients. *International Journal for Uncertainty Quantification*, 5(1):49–72, 2015.
- [43] P. G. Constantine, M. Emory, J. Larsson, and G. Iaccarino. Exploiting active subspaces to quantify uncertainty in the numerical simulation of the HyShot II scramjet. *Journal of Computational Physics*, 302:1–20, 12 2015.
- [44] Paul G. Constantine, Carson Kent, and Tan Bui-Thanh. Accelerating Markov chain Monte Carlo with active subspaces. *SIAM Journal on Scientific Computing*, 38(5):A2779–A2805, 2016.
- [45] Marco Tezzele, Filippo Salmoiraghi, Andrea Mola, and Gianluigi Rozza. Dimension reduction in heterogeneous parametric spaces with application to naval engineering shape design problems. *Advanced Modeling and Simulation in Engineering Sciences*, 5(1), 2018.
- [46] James C. Gross, Pranay Seshadri, and Geoff Parks. Optimisation with Intrinsic Dimension Reduction: A Ridge Informed Trust-Region Method. In *AIAA Scitech 2020 Forum*, pages 1–21, 2020.
- [47] Nicola Demo, Marco Tezzele, and Gianluigi Rozza. A supervised learning approach involving active subspaces for an efficient genetic algorithm in high-dimensional optimization problems. *arXiv preprint arXiv:2006.07282*, pages 1–21, 2020.
- [48] Olivier Zahm, Paul G. Constantine, Clémentine Prieur, and Youssef M. Marzouk. Gradient-based dimension reduction of multivariate vector-valued functions. *SIAM Journal on Scientific Computing*, 42(1):A534–A558, 2020.
- [49] Dushhyanth Rajaram, Raphael H Gautier, Christian Perron, Olivia J Pinon-Fischer, and Dimitri Mavris. Non-Intrusive Parametric Reduced Order Models with High-Dimensional Inputs via Gradient-Free Active Subspace. In *AIAA Aviation 2020 Forum*, page 3184, 2020.
- [50] Remi R. Lam, Olivier Zahm, Youssef M. Marzouk, and Karen E. Willcox. Multifidelity dimension reduction via active subspaces. *SIAM Journal on Scientific Computing*, 42(2):A929–A956, 2020.
- [51] Trent Michael Russi. *Uncertainty Quantification with Experimental Data and Complex System Models*. PhD thesis, UC Berkeley, 2010.
- [52] Steven H. Berguin, David Rancourt, and Dimitri N. Mavris. Method to facilitate high-dimensional design space exploration using computationally expensive analyses. *AIAA Journal*, 53(12):3752–3765, 12 2015.
- [53] Pranay Seshadri, Shaowu Yuchi, and Geoffrey T. Parks. Dimension reduction via Gaussian ridge functions. *SIAM-ASA Journal on Uncertainty Quantification*, 7(4):1301–1322, 2 2019.
- [54] Ramakrishna Tipireddy and Roger Ghanem. Basis adaptation in homogeneous chaos spaces. *Journal of Computational Physics*, 259:304–317, 2014.

- [55] Mark Girolami, Ben Calderhead, and Siu A. Chin. Riemannian Manifold Hamiltonian Monte Carlo. *arXiv preprint arXiv:0907.1100*, 2009.
- [56] Simon Byrne and Mark Girolami. Geodesic Monte Carlo on embedded manifolds. *Scandinavian Journal of Statistics*, 40(4):825–845, 2013.
- [57] Ron Shepard, Gergely Gidofalvi, and Scott R. Brozell. The multifacet graphically contracted function method. II. A general procedure for the parameterization of orthogonal matrices and its application to arc factors. *Journal of Chemical Physics*, 141(6), 2014.
- [58] Rajbir S. Nirwan and Nils Bertschinger. Rotation invariant householder parameterization for Bayesian PCA. *36th International Conference on Machine Learning, ICML 2019*, 2019-June:8466–8474, 2019.
- [59] Michael Jauch, Peter D. Hoff, and David B. Dunson. Monte Carlo simulation on the Stiefel manifold via polar expansion. *arXiv preprint arXiv:1906.07684*, 2019.
- [60] Arya A Pourzanjani, Richard M Jiang, Brian Mitchell, Paul J Atzberger, and Linda R Petzold. Bayesian Inference over the Stiefel Manifold via the Givens Representation. *arXiv preprint arXiv:1710.09443*, 2017.
- [61] Rohit K. Tripathy and Ilias Bilonis. Deep UQ: Learning deep neural network surrogate models for high dimensional uncertainty quantification. *Journal of Computational Physics*, 375:565–588, 2018.
- [62] M. J. Betancourt. Generalizing the No-U-Turn Sampler to Riemannian Manifolds. *arXiv preprint arXiv:1304.1920*, 2013.
- [63] Panagiotis Tsilifis, Piyush Pandita, Sayan Ghosh, Valeria Andreoli, Thomas Vandeputte, and Liping Wang. Bayesian learning of orthogonal embeddings for multi-fidelity Gaussian Processes. *arXiv preprint arXiv:2008.02386*, pages 1–23, 2020.
- [64] Christopher K I Williams and Carl Edward Rasmussen. *Gaussian processes for machine learning*, volume 2. MIT press Cambridge, MA, 2006.
- [65] Paul G. Constantine. *Active Subspaces: Emerging Ideas for Dimension Reduction in Parameter Studies*. Society for Industrial and Applied Mathematics, 3 2015.
- [66] James Townsend, Niklas Koep, and Sebastian Weichwald. Pymanopt: A python toolbox for optimization on manifolds using automatic differentiation. *Journal of Machine Learning Research*, 17:1–5, 2016.
- [67] Eli Bingham, Jonathan P. Chen, Martin Jankowiak, F. Obermeyer, Neeraj Pradhan, Theofanis Karaletsos, Rohit Singh, Paul Szerlip, Paul Horsfall, and Noah D. Goodman. Pyro: Deep universal probabilistic programming. *Journal of Machine Learning Research*, 20(1):973–978, 2019.
- [68] Yanyuan Ma and Liping Zhu. A review on dimension reduction. *International Statistical Review*, 81(1):134–150, 2013.
- [69] Paul G. Constantine, Armin Eftekhari, Jeffrey Hokanson, and Rachel A. Ward. A near-stationary subspace for ridge approximation. *Computer Methods in Applied Mechanics and Engineering*, 326:402–421, 2017.
- [70] Nathan Wycoff, Mickael Binois, and Stefan M. Wild. Sequential Learning of Active Subspaces. *arXiv preprint arXiv:1907.11572*, pages 1–33, 2019.
- [71] Du Phan, Neeraj Pradhan, and Martin Jankowiak. Composable Effects for Flexible and Accelerated Probabilistic Programming in NumPyro. *arXiv preprint arXiv:1912.11554*, pages 1–10, 2019.
- [72] James Bradbury, Roy Frostig, Peter Hawkins, Matthew James Johnson, Chris Leary, Dougal Maclaurin, and Skye Wanderman-Milne. {JAX}: composable transformations of {P}ython+{N}um{P}y programs, 2018.
- [73] Tyson Loudon and Stephen Pankavich. Mathematical analysis and dynamic active subspaces for a long term model of HIV. *Mathematical Biosciences and Engineering*, 14(3):709–733, 2017.
- [74] Trent W Lukaczyk, Paul Constantine, Francisco Palacios, and Juan J Alonso. Active Subspaces for Shape Optimization. In *10th AIAA multidisciplinary design optimization conference*, page 1171, 2014.
- [75] A.V. Knyazev and P. Zhu. Principal Angles Between Subspaces and Their Tangents. *Mitsubishi Electric Research Laboratories*, 2012.

Appendix A. Numerical Values Truncated from Figure 7 for readability

Repetition	Method	Number of Training Samples				
		30	60	90	120	150
1	B-AS	-0.38	-0.25	-3.55	0.83	0.58
	MO-AS	-2.85	-2.73	-2.35	-1.64	-1.54
	B-GP	-1.46	-1.41	-0.83	-0.76	-0.63
2	B-AS	-0.60	-3.87	-0.82	-0.05	0.64
	MO-AS	-2.06	-2.34	-2.65	-2.09	-1.73
	B-GP	-1.44	-1.45	-0.77	-0.70	-0.70
3	B-AS	-0.50	-13.48	-0.27	0.52	1.05
	MO-AS	-2.88	-1.87	-2.16	-1.59	-1.89
	B-GP	-1.41	-1.46	-1.17	-0.75	-0.70
4	B-AS	-0.62	0.20	-22.67	0.72	0.90
	MO-AS	-2.65	-2.57	-1.98	-1.85	-1.76
	B-GP	-1.48	-1.44	-0.86	-0.64	-0.63
5	B-AS	-0.14	-17.43	-2.41	0.81	-0.62
	MO-AS	-2.86	-2.98	-2.05	-1.76	-2.60
	B-GP	-1.45	-1.54	-0.98	-0.71	-0.60

Table 2: Validation posterior log-likelihood values truncated from Figure 7 to improve readability for the HIV dataset.